

Multi-fidelity data fusion through parameter space reduction with applications to automotive engineering

Francesco Romor^{*a}, Marco Tezzele^{†a}, Markus Mrosek^{‡b}, Carsten Othmer^{§b}, and
Gianluigi Rozza^{¶a}

^aMathematics Area, mathLab, SISSA, via Bonomea 265, I-34136 Trieste, Italy

^bVolkswagen AG, Innovation Center Europe, 38436 Wolfsburg, Germany

October 28, 2021

Abstract

Multi-fidelity models are of great importance due to their capability of fusing information coming from different simulations and sensors. Gaussian processes are employed for non-parametric regression in a Bayesian setting. They generalize linear regression embedding the inputs in a latent manifold inside an infinite-dimensional reproducing kernel Hilbert space. We can augment the inputs with the observations of low-fidelity models in order to learn a more expressive latent manifold and thus increment the model's accuracy. This can be realized recursively with a chain of Gaussian processes with incrementally higher fidelity. We would like to extend these multi-fidelity model realizations to case studies affected by a high-dimensional input space but with low intrinsic dimensionality. In these cases physical supported or purely numerical low-order models are still affected by the curse of dimensionality when queried for responses. When the model's gradient information is provided, the existence of an active subspace, or a nonlinear transformation of the input parameter space, can be exploited to design low-fidelity response surfaces and thus enable Gaussian process multi-fidelity regression, without the need to perform new simulations. This is particularly useful in the case of data scarcity. In this work we present a new multi-fidelity approach involving active subspaces and nonlinear level-set learning method. We test the proposed numerical method on two different high-dimensional benchmarks, and on a more complex car aerodynamics problem. We show how a low intrinsic dimensionality bias can increase the accuracy of GP response surfaces.

1 Introduction

Every day more and more complex simulations are made possible thanks to the high-performance computing facilities spread and to the advancements in computational methods. Still the study and the approximation of high-dimensional functions of interest represent a problem due to the curse of dimensionality and the data scarcity because of limited computation budgets.

Gaussian processes (GP) [54] have been proved as a versatile and powerful technique for regression (GPR), classification, inverse problem resolution, and optimization, among others. In the last years several studies and extensions have been proposed in the context of non-parametric and interpretable Bayesian models. For a review on Gaussian processes and kernel methods we suggest [20], while for approximation methods in the framework of GP see [37]. Progress has also been made to deal with big data and address some memory limitations of GPR, as for example by sparsifying the spectral representation of the GP [25] or introducing stochastic variational inference for GP models [28].

At the same time, multi-fidelity modelling has been proven effective in a heterogeneous set of applications [21, 14, 38, 3, 4, 23], where expensive but accurate high-fidelity measurements

*francesco.romor@sissa.it

†marco.tezzele@sissa.it

‡markus.mrosek@volkswagen.de

§carsten.othmer@volkswagen.de

¶gianluigi.rozza@sissa.it

are coupled with cheaper to compute and less accurate low-fidelity data. Recent advancements have been made for nonlinear autoregressive multi-fidelity Gaussian process regression (NARGP), as proposed in [36], and with physics informed neural networks (PINNs) [39] in the context of multi-fidelity approximation in [30].

The increased expressiveness of these models is achieved thanks to some kind of nonlinear approach that extend GP models to non-GP processes with the disadvantage of an additional computational cost. In this direction are focused the following works which aim to obtain computationally efficient heteroscedastic GP models with a variational inference approach [26] or employing a nonlinear transformation [47]. This approach is extended to multi-fidelity models departing from the linear formulation of Kennedy and O’Hagan [21] towards deep Gaussian processes [9] and NARGP.

When the models depend on a high-dimensional input space even the low-fidelity approximations supported by a physical interpretation or a purely numerical model order reduction suffer from the curse of dimensionality especially for the design of high-dimensional GP models. Active subspaces (AS) [7, 55] can be used to build a surrogate low-fidelity model with reduced input space taking advantage of the correlations of the model’s gradients when available. Reduction in parameter space through AS has been proven successful in a diverse range of applications such as: shape optimization [29, 15, 12, 10], car aerodynamics studies [33], hydrologic models [19], naval and nautical engineering [51, 31], coupled with intrusive reduced order methods in cardiovascular studies [48], in CFD problems in a data-driven setting [11, 50]. A kernel-based extension of AS for both scalar and vectorial functions can be found in [40], while for a new local approach to parameter space reduction see [41].

Linked to Active Manifolds [5], another technique for dimension reduction in the parameter space is Nonlinear Level-set Learning (NLL) [56], which implements Reversible Neural Networks (RevNet) to learn a chart of the graph of the objective function that parametrizes the level-sets.

The aim of the present contribution is to propose a multi-fidelity regression model which exploits the intrinsic dimensionality of high-dimensional functions of interest and the presence of an active subspace or nonlinear active subspace to reduce the approximation error of high-fidelity response surfaces. Our approach employs the design of a NARGP using an AS/NLL response surface as low-fidelity model. We follow the preliminary studies conducted in [43]. In the literature the multi-fidelity approximation paradigm has been adopted in a different way to search for an active subspace from given high- and low-fidelity models in [24].

The outline of this work is the following: in Section 2 we present the general framework of Gaussian process regression and in particular the NARGP multi-fidelity approach; in Section 3 we briefly present the active subspaces property and the nonlinear level-set learning method we are going to exploit as low-fidelity models, together with some error estimates for the construction of response surfaces; Section 4 is devoted to present how data fusion with active subspaces and nonlinear level-set learning is performed with the aid of pseudocode; in Section 5 we apply the proposed approach to the piston and Ebola benchmark models, and to an automotive application, showing the better performance achieved by the multi-fidelity regression; finally in Section 6 we present our conclusions and we draw some future perspectives.

2 Multi-fidelity Gaussian process regression

In this section we are going to present the Gaussian process regression (GPR) [54] technique which is the main ingredient for the construction of multi-fidelity GPR, and the nonlinear autoregressive multi-fidelity Gaussian process regression (NARGP) introduced in [36], which we are going to exploit for our proposed multi-fidelity method. All these techniques are presented in the general setting considering multiple levels of fidelity.

2.1 Gaussian process regression

Gaussian process regression is a supervised technique to approximate unknown functions given a finite set of input/output pairs $\mathcal{S} = \{x_i, y_i\}_{i=1}^N$. Let $f : \mathcal{X} \subset \mathbb{R}^m \rightarrow \mathbb{R}$ be the scalar function of interest. The set \mathcal{S} is generated through f with the following relation: $y_i = f(x_i)$, which are the noise-free observations. We assigned a prior to f with mean $m(\mathbf{x})$ and covariance function $k(\mathbf{x}, \mathbf{x}'; \theta)$, that is $f(\mathbf{x}) \sim \mathcal{GP}(m(\mathbf{x}), k(\mathbf{x}, \mathbf{x}'; \theta))$. The prior expresses our beliefs about the function before looking at the observed values. From now on we consider zero mean \mathcal{GP} , that is $m(\mathbf{x}) = \mathbf{0}$, and we define the covariance matrix as $\mathbf{K}_{i,j} = k(x_i, x_j; \theta)$, with $\mathbf{K} \in \mathbb{R}^{N \times N}$. In order to make

predictions using the Gaussian process we still need to find the optimal values for the hyper-parameters vector θ by maximizing the log likelihood:

$$\log p(\mathbf{y}|\mathbf{x}, \theta) = -\frac{1}{2}\mathbf{y}^T \mathbf{K}^{-1} \mathbf{y} - \frac{1}{2} \log |\mathbf{K}| - \frac{N}{2} \log 2\pi. \quad (1)$$

Let \mathbf{x}_* be the test samples, and $\mathbf{K}_{N^*} = k(\mathbf{x}, \mathbf{x}_*; \theta)$ be the matrix of the covariances evaluated at all pairs of training and test samples, and in a similar fashion $\mathbf{K}_{*N} = k(\mathbf{x}_*, \mathbf{x}; \theta)$, and $\mathbf{K}_{**} = k(\mathbf{x}_*, \mathbf{x}_*; \theta)$. By conditioning the joint Gaussian distribution on the observed values we obtain the predictions f_* by sampling the posterior as

$$f_* | \mathbf{x}_*, \mathbf{x}, \mathbf{y} \sim \mathcal{N}(\mathbf{K}_{*N} \mathbf{K}^{-1} \mathbf{y}, \mathbf{K}_{**} - \mathbf{K}_{*N} \mathbf{K}^{-1} \mathbf{K}_{N^*}). \quad (2)$$

2.2 Nonlinear multi-fidelity Gaussian process regression

In this section we briefly present the nonlinear autoregressive multi-fidelity Gaussian process regression (NARGP) scheme proposed in [36]. It extends the concepts present in [21, 27] to nonlinear correlations between the different available fidelities.

The procedure is purely data-driven. We start from the input/output pairs corresponding to p levels of increasing fidelity, that is

$$\mathcal{S}_q = \{x_i^q, y_i^q\}_{i=1}^{N_q} \subset \mathcal{X} \times \mathbb{R} \subset \mathbb{R}^m \times \mathbb{R}, \quad \text{for } q \in \{1, \dots, p\}, \quad (3)$$

where $y_i^q = f_q(x_i^q)$. With p we indicate the highest fidelity. We also assume that the design sets have a hierarchical structure:

$$\pi(\mathcal{S}_p) \subset \pi(\mathcal{S}_{p-1}) \subset \dots \subset \pi(\mathcal{S}_1), \quad (4)$$

where $\pi : \mathbb{R}^m \times \mathbb{R} \rightarrow \mathbb{R}^m$ is the projection onto the first m coordinates. Due to this hierarchy, when the fidelities of the available datasets cannot be neatly assessed, it is reasonable to consider the cost needed to produce them as ordering criterion, see Remark 3.

The NARGP formulation assigns a Gaussian process to each fidelity model f_q , so they are completely defined by the mean field m_q , with the constant zero field as prior, and by their kernel k_q , as follows:

$$y_q(\bar{x}) - \epsilon \sim \mathcal{GP}(f_q(\bar{x}) | m_q(\bar{x}), k_q(\theta_q)) \quad \forall q \in \{1, \dots, p\}, \quad (5)$$

where $\epsilon \sim \mathcal{N}(0, \sigma^2)$ is a noise term and

$$\bar{x} := \begin{cases} (\mathbf{x}, f_{q-1}(\mathbf{x})) \in \mathbb{R}^d \times \mathbb{R}, & q > 1 \\ \mathbf{x} \in \mathbb{R}^d, & q = 1 \end{cases}. \quad (6)$$

The definition of the kernel $k_q(\theta_q)$ implements the auto-regressive characteristic of the method since it depends on the previous fidelity model f_{q-1} :

$$k_q((x, f_{q-1}(x)), (x', f_{q-1}(x')) | \theta_q) = k_q^\rho(x, x'; \theta_q^\rho) \cdot k_q^f(f_{q-1}(x), f_{q-1}(x'); \theta_q^f) + k_q^\delta(x, x'; \theta_q^\delta). \quad (7)$$

The hyper-parameters to be tuned are represented by $\theta_q \equiv (\theta_q^\rho, \theta_q^f, \theta_q^\delta)$ and are associated respectively to the multiplicative kernel k_q^ρ , the auto-regressive kernel k_q^f , and the kernel k_q^δ , which corresponds to the non auto-regressive part in the sum of Equation 7. For our applications we employ the radial basis function kernel with automatic relevance determination (RBF-ARD) [54], but there are other possible choices. With this scheme, we can formally infer the high-fidelity response by learning the latent nonlinear manifold that relates the inputs, the lower fidelity posterior and the high-fidelity posterior [36]. This structure allows for nonlinear and more general cross-correlations between subsequent fidelities than just a linear auto-regressive multi-fidelity scheme.

A part from the first level of fidelity $q = 1$ the posterior probability distribution given the previous fidelity models is no longer Gaussian since the inputs are couples $((\mathbf{x}, \mathbf{x}_*), (y_{q-1}(\mathbf{x}), f_{q-1}^{\text{post}}(\mathbf{x}_*)))$ where f_{q-1}^{post} is a Gaussian process. We used the notation $(\mathbf{x}, y_{q-1}(\mathbf{x}))$ for the training set and \mathbf{x}_* for the new input. So in order to evaluate the predictive mean and variance for a new input \mathbf{x}_* we have to integrate the posterior $p(f_q(\mathbf{x}_*) | f_{q-1}, \mathbf{x}_*, \mathbf{x}_q, y_q)$ as

$$f_q(\mathbf{x}_* | f_{q-1}, \mathbf{x}_*, \mathbf{x}_q, y_q) \sim \mathcal{N}(\mathbf{K}_{*N}^q (\mathbf{K}^q)^{-1} y_q, \mathbf{K}_{**}^q - \mathbf{K}_{*N}^q (\mathbf{K}^q)^{-1} \mathbf{K}_{N^*}^q), \quad (8)$$

$$\mathbf{K}_{*N}^q = k_q((\mathbf{x}_*, f_{q-1}(\mathbf{x}_*)), (\mathbf{x}_{q-1}, y_{q-1}); \theta_q), \quad (9)$$

$$\mathbf{K}_{N^*}^q = k_q((\mathbf{x}_{q-1}, y_{q-1}), (\mathbf{x}_*, f_{q-1}(\mathbf{x}_*)); \theta_q), \quad (10)$$

$$\mathbf{K}^q = k_q((\mathbf{x}_{q-1}, y_{q-1}), (\mathbf{x}_{q-1}, y_{q-1}); \theta_q), \quad (11)$$

over the Gaussian distribution of the prediction at the previous level $f_{q-1}(\mathbf{x}_*) \sim \mathcal{N}(m_q(\mathbf{x}_*), k_q(\mathbf{x}_*))$. In practice the following integral is approximated with recursive Monte Carlo at each fidelity level, for all $q \in \{2, \dots, p\}$,

$$p(f_q^{\text{post}}(\mathbf{x}_*)) := p(f_q(\mathbf{x}_*) | f_{q-1}, \mathbf{x}_*, \mathbf{x}_q, y_q) = \int_{\mathcal{X}} p(f_q(\mathbf{x}_*) | s, \mathbf{x}_*, \mathbf{x}_q, y_q) d\mathcal{L}_{f_{q-1}^{\text{post}}(\mathbf{x}_*)}(s) \quad (12)$$

$$p(f_1^{\text{post}}(\mathbf{x}_*)) := p(f_1(\mathbf{x}_*) | \mathbf{x}_*, \mathbf{x}_1, y_1) \sim \mathcal{N}(m_1(\mathbf{x}_*), k_1(\mathbf{x}_*)), \quad (13)$$

where $\mathcal{L}_{f_{q-1}^{\text{post}}(\mathbf{x}_*)}$ is the probability law of $f_{q-1}^{\text{post}}(\mathbf{x}_*) \sim \mathcal{N}(m_q(\mathbf{x}_*), k_q(\mathbf{x}_*))$. In the applications we always use 200 Monte Carlo samples, since the results do not vary much increasing them.

The hyper-parameters θ_q are optimized (non recursively) with maximum log-likelihood estimation for each GP model $\mathcal{GP}(f_q | \mathbf{0}, k^q(\theta_q))$, for all $q \in \{1, \dots, p\}$,

$$\underset{\theta_q}{\text{argmin}} -\log p(f_q(\mathbf{x}_q) | \mathbf{x}_q, y_q, y_{q-1}, \theta_q) \propto \frac{1}{2} \log |K^q(\theta_q)| + \frac{1}{2} y_q^T (K^q(\theta_q))^{-1} y_q, \quad (14)$$

this is why a hierarchical dataset is needed. The hyperparameters tuning is achieved maximizing the log-likelihood with the gradient descent optimizer L-BFGD in GPy [16]. For some test cases, the training procedure is subject to relevant perturbations relative to the number of restarts, this is especially true in higher dimensions of the parameter space as in the Ebola 3 and Jetta-12 10 test cases, with 8 and 12 parameters respectively.

3 Parameter space reduction

Our aim is testing multi-fidelity Gaussian process regression models to approximate objective functions which depend on inputs sampled from a high-dimensional space. Low-fidelity models relying on a physical supported or numerical model reduction — for example a coarse discretization or a more specific numerical model order reduction — still suffer from the high dimensionality of the input space.

In our approach we try to tackle these problematics by searching for a surrogate (low-fidelity) model accounting for the complex correlations among the input parameters that concur to the output of interest. With this purpose in mind in this section we are going to briefly present the active subspaces (AS) property [7], and the nonlinear level-set learning (NLL) method [56] for parameter space reduction in order to design response surfaces with Gaussian process regression.

3.1 Active subspaces

Let the inputs be represented by an absolutely continuous random variable \mathbf{X} with probability density ρ such that $\text{supp}(\rho) = \mathcal{X} \subset \mathbb{R}^m$, where m is the dimension of the input space. If our numerical simulations provide also the gradients of the samples for which the model is inquired for, we can approximate the correlation matrix of the gradient with simple Monte Carlo as

$$\mathbb{E}_\rho[\nabla_{\mathbf{x}} f (\nabla_{\mathbf{x}} f)^T] \approx \frac{1}{N} \sum_{i=1}^N \nabla_{\mathbf{x}} f(\mathbf{X}_i) (\nabla_{\mathbf{x}} f(\mathbf{X}_i))^T, \quad (15)$$

where N is the number of samples. We are looking for the highest spectral gap $\lambda_r - \lambda_{r+1}$ in the sequence of ordered eigenvalues of the approximated correlation matrix, that is

$$\lambda_1 \geq \dots \geq \lambda_r \geq \lambda_{r+1} \geq \dots \geq \lambda_m. \quad (16)$$

The active subspace is the eigenspace corresponding to the eigenvalues $\lambda_1, \dots, \lambda_r$ and we represent it with the matrix $\hat{W}_1 \in \mathcal{M}(m \times r)$ which columns are the first r active eigenvectors. Then the response surface \mathcal{R} is built with a Gaussian process regression over the training set composed by N_{train} input-output pairs $\{W_1^T \mathbf{x}_i, y_i\}_{i=1}^{N_{\text{train}}}$.

An a priori bound on the error can be proved [7], but the whole approximation procedure considers additional steps for the evaluation of the optimal profile $\mathbb{E}_\rho[f | \hat{W}_1^T \mathbf{X}]$ and its approximation with Monte Carlo $\overline{\mathbb{E}_\rho[f | \hat{W}_1^T \mathbf{X}]}$:

$$f(\mathbf{X}) \approx \mathbb{E}_\rho[f | \hat{W}_1^T \mathbf{X}] \approx \overline{\mathbb{E}_\rho[f | \hat{W}_1^T \mathbf{X}]} \approx \mathcal{R}(\hat{W}_1 \mathbf{X}). \quad (17)$$

The mean square regression error is bounded a priori by

$$\mathbb{E}_\rho \left[(f(\mathbf{X}) - \mathcal{R}(\hat{W}_1^T \mathbf{X}))^2 \right] \leq C_1 (1 + N^{-1/2})^2 \left(\epsilon (\lambda_1 + \dots + \lambda_r)^{1/2} + (\lambda_{r+1} + \dots + \lambda_m)^{1/2} \right)^2 + C_2 \delta,$$

where C_1 and C_2 are constants, ϵ quantifies the error in the approximation of the true active subspace W_1 with \hat{W}_1 obtained from the Monte Carlo approximation, and $C_2 \delta$ is a uniform bound.

3.2 Nonlinear level-set learning method

This method seeks a bijective nonlinear transformation $g_{\text{NLL}} : \mathcal{X} \rightarrow \tilde{\mathcal{X}} \subset \mathbb{R}^m$ to capture the geometry of level sets and parametrize them in a low-dimensional space. To this end in [56] they employ reversible networks (RevNets) [6] to learn the transformation g_{NLL} . The designed loss function uses samples of the gradients of the target function to encourage the transformed function to be sensitive to only a few active coordinates. In [17] they introduce a variation of such loss function in the context of PDEs.

To construct the RevNet they use the following architecture [18], which is reversible by definition:

$$\begin{cases} u_{n+1} = u_n + h K_{n,1}^T \sigma(K_{n,1} v_n + b_{n,1}), \\ v_{n+1} = v_n - h K_{n,2}^T \sigma(K_{n,2} u_n + b_{n,2}), \end{cases} \quad \text{for } n = 0, 1, \dots, N-1, \quad (18)$$

where u and v are partitions of the states, h is a scalar time step, the matrices K contain the weights, b represent the biases, and σ is the activation function. We remark that the original coordinates and the transformed ones are split in two in u and v .

4 Multi-fidelity data fusion with active subspaces

Our study is based on the design of a nonlinear autoregressive multi-fidelity Gaussian process regression (NARGP) [36] whose low-fidelity level is learnt from a response surface built through a parameter space reduction technique — here we focus on active subspaces but little modifications are required in order to use NLL as we are going to show. We suppose that the model in consideration has indeed a high dimensional input space but its intrinsic dimensionality is sufficiently lower. This is often the case as shown by the numerous industrial applications [33, 49, 51, 29].

The incorporation of prior knowledge, biasing the learning process, is inevitable for the success of learning algorithms. In our methodology this is realized in two ways: with the kernel of the Gaussian process (type of spatial correlations, degree of smoothness of the model) and with the low-fidelity intrinsic dimensionality assumption (presence of a dominant linear or nonlinear active subspace). In Figure 1 we present an illustrative scheme of the proposed NARGP-AS method.

The whole procedure requires the knowledge of an input/output high-fidelity training set $\{(\mathbf{x}_i^H, y_i^H)\}_{i=1}^{N_H} \subset \mathbb{R}^m \times \mathbb{R}$, completed by the gradients $\{dy_i^H\}_{i=1}^{N_H} \subset \mathbb{R}^m$ (eventually approximated from the input/output dataset) needed for the active subspace’s presence inquiry, and a low-fidelity input set $\{\mathbf{x}_i^L\}_{i=1}^{N_L} \subset \mathbb{R}^m$. We represent with N_H, N_L the number of high-fidelity and low-fidelity training set samples, respectively. Differently from the usual procedure the low-fidelity outputs $\{y_i^L\}_{i=1}^{N_L}$ are predicted with the response surface built thanks to the presence of the active subspace using the dataset $\{(\hat{W}_1 \mathbf{x}_i^H, y_i^H)\}_{i=1}^{N_H}$. At the same time the response surface is also queried for the predictions $\{y_i^{H,\text{train}}\}_{i=1}^{N_H}$ at the high-fidelity inputs $\{\mathbf{x}_i^H\}_{i=1}^{N_H}$ that will be used for the training of the multi-fidelity model. Now all the ingredients for the procedure described in [36] are ready: the multi-fidelity model is trained at the low-fidelity level with $\{(x_i^L, y_i^L)\}_{i=1}^{N_L}$ and at the high-fidelity level with $\{(x_i^H, y_i^{H,\text{train}}), y_i^H\}_{i=1}^{N_H}$.

We remark that in this case the same high-fidelity outputs $\{y_i^H\}_{i=1}^{N_H} \subset \mathbb{R}$ are used for the response surface training and the high-fidelity training of the multi-fidelity model. In fact the outputs $\{y_i^{H,\text{train}}\}_{i=1}^{N_H}$ predicted with the response surface are equal to $\{y_i^H\}_{i=1}^{N_H} \subset \mathbb{R}$ since the response surface is a Gaussian process with no noise (at least theoretically, see Remark 2) trained on the dataset $\{(\hat{W}_1 \mathbf{x}_i^H, y_i^H)\}_{i=1}^{N_H}$ and queried for the same inputs $\{\hat{W}_1 \mathbf{x}_i^H\}_{i=1}^{N_H}$ for the predictions, that is $\{y_i^{H,\text{train}}\}_{i=1}^{N_H}$. This results in the training of the high-fidelity level of the multi-fidelity model with the dataset $\{((x_i^H, y_i^{H,\text{train}}), y_i^H)\}_{i=1}^{N_H} = \{(x_i^H, y_i^H), y_i^H\}_{i=1}^{N_H}$.

We expect that with the multi-fidelity approach, thanks to the nonlinear fidelity fusion realized by the method, not only the lower accuracy of the low-fidelity model will be safeguarded against,

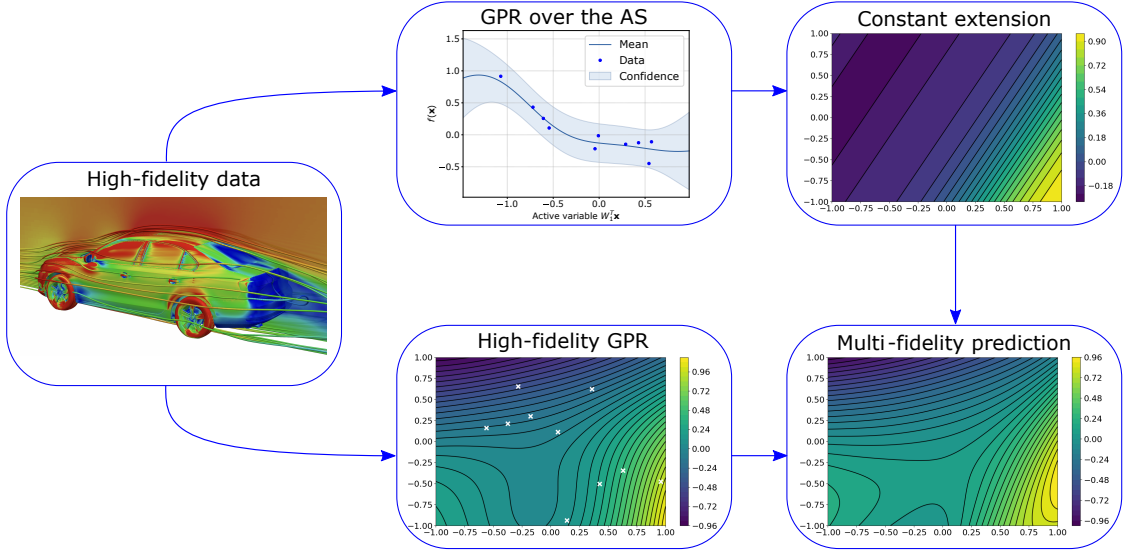


Figure 1: Illustrative scheme of the NARGP-AS method. Starting from 10 high-fidelity data (depicted in blue and in white) we construct as low-fidelity model a response surface which is constant along the inactive subspace.

but also a hint towards the presence of an active subspace will be transferred from the low-fidelity to the high-fidelity level. In fact the low-fidelity GP regression model is built from the predictions obtained with the r -dimensional response surface which expressiveness is guaranteed by the additional assumption that the model under investigation has a r -dimensional active subspace. So, a part from the lower computational budget and the reduced accuracy, our low-fidelity model should transfer to the high-fidelity level the knowledge of the presence of an active subspace when learning correlations among the inputs $\{x_i^H\}_{i=1}^{N_H}$, the response surfaces predictions $\{y_i^{H,\text{train}}\}_{i=1}^{N_H}$ and the high-fidelity targets $\{y_i^H\}_{i=1}^{N_H}$. The overhead with respect to the original procedure [36] is the evaluation of the active subspace from the high-fidelity inputs and the training of the whole multi-fidelity model. The procedure is synthetically reviewed through Algorithm 1.

Remark 1 (Nonlinear level-set learning as LF model). If NLL is employed to build the low-fidelity level, only the first step of Algorithm 1 is changed. For our applications, the GPR designed with NLL has dimension one.

Algorithm 1: NARGP-AS response surface design algorithm.

input : high-fidelity inputs, outputs, gradients triplets

$$\{(\mathbf{x}_i^H, y_i^H, dy_i^H)\}_{i=1}^{N_H} \subset \mathbb{R}^m \times \mathbb{R} \times \mathbb{R}^m,$$

low-fidelity inputs $\{\mathbf{x}_i^L\}_{i=1}^{N_L} \subset \mathbb{R}^m,$

test dataset $\{(\mathbf{x}_i^{\text{test}}, y_i^{\text{test}})\}_{i=1}^{N_{\text{test}}},$

output: multi-fidelity model,

$$\left((f_H | x_i^H, y_i^{H,\text{train}}), (f_L | x_i^L) \right) \sim (\mathcal{GP}(f_H | m_H, k_H), \mathcal{GP}(f_L | m_L, k_L))$$

- 1 Compute the active subspace \hat{W}_1 with the high-fidelity gradients $\{dy_i^H\}_{i=1}^{N_H}$,
 - 2 Build the one-dimensional response surface $\mathcal{R}(\hat{W}_1 \mathbf{X})$ with a GP regression from $\{(\hat{W}_1 \mathbf{x}_i^H, y_i^H)\}_{i=1}^{N_H}$,
 - 3 Predict the low-fidelity outputs $\{y_i^L\}_{i=1}^{N_L}$ at $\{\mathbf{x}_i^L\}_{i=1}^{N_L}$ and the training high-fidelity inputs $\{y_i^{H,\text{train}}\}_{i=1}^{N_H}$ at $\{\mathbf{x}_i^H\}_{i=1}^{N_H}$ with the response surface,
 - 4 Train the multi-fidelity model at the low-fidelity level f_L with the training dataset $\{(x_i^L, y_i^L)\}_{i=1}^{N_L} \cup \{(x_i^H, y_i^{H,\text{train}})\}_{i=1}^{N_H}$,
 - 5 Train the multi-fidelity model at the high-fidelity level f_H with the training dataset $\{(x_i^H, y_i^{H,\text{train}}), y_i^H\}_{i=1}^{N_H}$
-

Remark 2 (Markov property). Theoretically the observations $\{y_i^q\}$ should be noiseless for each level of fidelity q in order to preserve the Markov property [36]. However in practice could be beneficial in some applications to add noise at each fidelity level.

5 Numerical results

In this section we are going to present the results obtained with the NARGP-AS and the NARGP-NLL method over two benchmark test problems, and over a more complex car aerodynamics problem. The library employed to implement the NARGP model is Emukit [34] while for the active subspace and NLL response surface design we used the open source Python package¹ called ATHENA [42] and GPy [16].

5.1 Benchmark test problems

We consider two different benchmark test problems for which a multi-fidelity model will be built. The first is a 7-dimensional model to compute the time it takes a cylindrical piston to complete a cycle² and the second is a 8-dimensional model for the spread of Ebola [13].

These tests have already been analyzed for the presence of an active subspace and they indeed present a low intrinsic dimensionality. For each model we show the sufficient summary plot along the one-dimensional active subspace found, and the correlation among the low-fidelity level and the high-fidelity level of the multi-fidelity model. We also present a comparison of the R^2 scores of the predictions with respect to a low-fidelity model (LF) represented by a GP regression on the low-fidelity input/output dataset, a high-fidelity model (HF) represented by a GP regression on the high-fidelity input/output dataset, and the proposed multi-fidelity model (MF). In each test case the number of low-fidelity samples is 200 and an error study over the number of high-fidelity samples used is undergone.

The piston model The algebraic cylindrical piston model appeared as a test for statistical screening in [2], while applications of AS to this model can be found in [8]. The scalar target function of interest is the time it takes the piston to complete a cycle, and its computation involves a chain of nonlinear functions. This quantity depends on 7 input parameters uniformly distributed. The corresponding variation ranges are taken from [8]. The 10000 test points are sampled with Latin hypercube sampling (LHS).

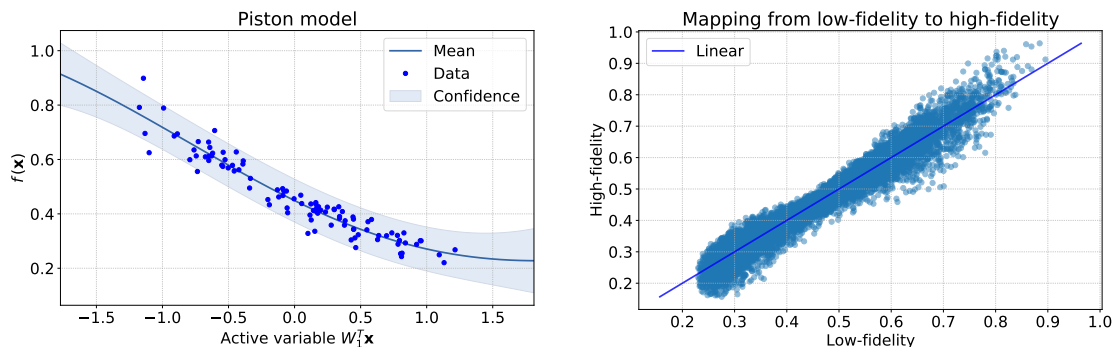


Figure 2: Left: sufficient summary plot of the surrogate model built with active subspaces. 100 samples were used to build the AS surrogate model shown. Right: correlation among the low-fidelity level and the high-fidelity level of the multi-fidelity model.

It is qualitatively evident from the sufficient summary plot in the left panel of Figure 2 that a one-dimensional active subspace is enough to explain with a fairly good accuracy the dependence of the output from the 7-dimensional inputs. This statement could be supported looking at the

¹Available at <https://github.com/mathLab/ATHENA>.

²The piston dataset was taken from https://github.com/paulcon/active_subspaces.

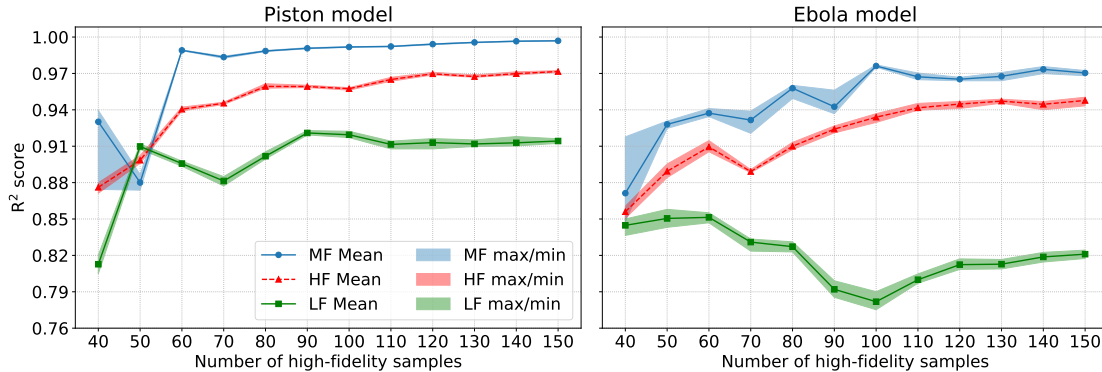


Figure 3: R^2 score of the posterior of the multi-fidelity (MF), high-fidelity (HF) and low-fidelity (LF) models against the number of high-fidelity samples used to find the active subspace and build the Gaussian process regressions of the MF, HF, LF models. The 10000 test samples are distributed with Latin hypercube sampling (LHS). In the left panel the results for the piston model, while on the right the Ebola spread model.

ordered eigenvalues of the correlation matrix of the gradients, which would show a spectral gap between the first and the second eigenvalue. We can also see in the right panel of Figure 2 the correlations scatter plot among the two different fidelity levels of the NARGP model.

Figure 3 shows on the left the mean R^2 scores of the MF model built as described in Section 4, over 10 training restarts of the MF, LF and HF models: moreover each GPR training is restarted 10 times for the HF and LF models and 20 times for the MF model at each fidelity level, inside the GPy package. We show also the minimum and maximum R^2 scores over the outer 10 training restarts to show the stability of the procedure. The relative gain is of approximately 3 – 5% with respect to the high-fidelity regression.

SEIR model for Ebola The SEIR model for the spread of Ebola depends on 8 parameters and the output of interest is the basic reproduction number R_0 . A complete AS analysis was made in [13], while a kernel-based active subspaces comparison can be found in [40]. The formulation is the following:

$$R_0 = \frac{\beta_1 + \frac{\beta_2 \rho_1 \gamma_1}{\omega} + \frac{\beta_3}{\gamma_2} \psi}{\gamma_1 + \psi}, \quad (19)$$

where the parameters range are taken from [13].

Differently from the previous test case, the one-dimensional response function in the left panel of Figure 4 does not explain well the model: in this case kernel-based active subspaces could be employed to reach a better expressiveness of the surrogate model [40]. Even the scatter plot in the right panel of Figure 4, which shows the correlations between the low-fidelity and high-fidelity levels of the NARGP model, exhibits a worse accuracy in the low-fidelity level with respect to the previous test case. These results are quantified in the right panel of Figure 3 with the R^2 score for the different fidelities models. We have reported the same quantities of the piston test case. The relative gain, also in this case, is approximately around 3 – 4% with respect to the high-fidelity regression.

From a comparison between the HF and MF models in Figure 3 it can be seen that the nonlinear autoregressive fidelity fusion approach learns relatively worse correlations of the low-/high-fidelity levels of the NARGP-AS Ebola model with respect to the piston model. For both the test cases the multi-fidelity regression approach with active subspaces results in better performance with a consistent reduction of the R^2 score over a test dataset of 10000 points.

5.2 Automotive application

Two different test cases from the world of automotive aerodynamics are investigated in order to demonstrate the applicability of the presented method to real-life problems. The first one (named hereafter **Jetta-6**) is taken from [32], where it is described in detail. It consists of a 6-dimensional

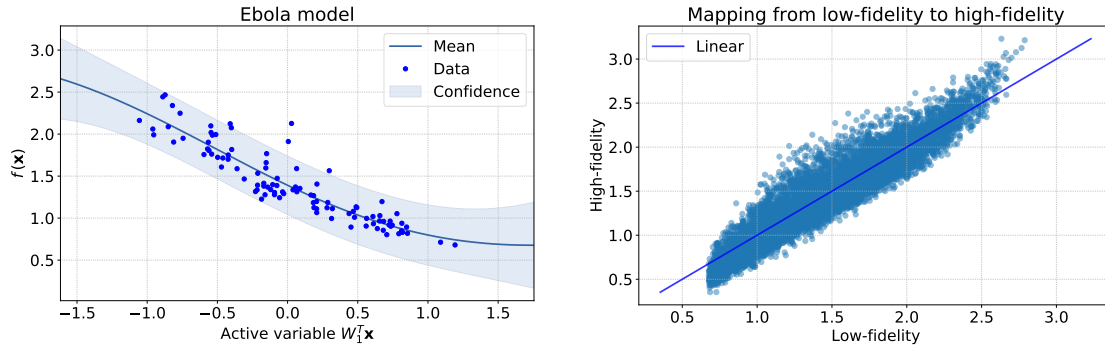


Figure 4: Left: sufficient summary plot of the Ebola model, 100 samples were used to build the AS surrogate model shown. Right: correlation among the low-fidelity level and the high-fidelity level of the multi-fidelity model.

geometric parameterization of the Volkswagen Jetta VI. The parameters (see Table 1) were generated by free-form deformation and focus on the rear part of the car. A Latin Hypercube with 101 samples was created, and the aerodynamic flow fields were computed with OpenFOAM [53] via Delayed Detached Eddy Simulations (DDES). An illustrative example can be seen in Figure 5. The physical simulation time was four seconds, and the fields were averaged over the last two seconds before integrating them over the vehicle surface to obtain the drag coefficient c_D . With mesh sizes being of the order of 100M cells, each variant required about 23,000 CPU-core-hours.

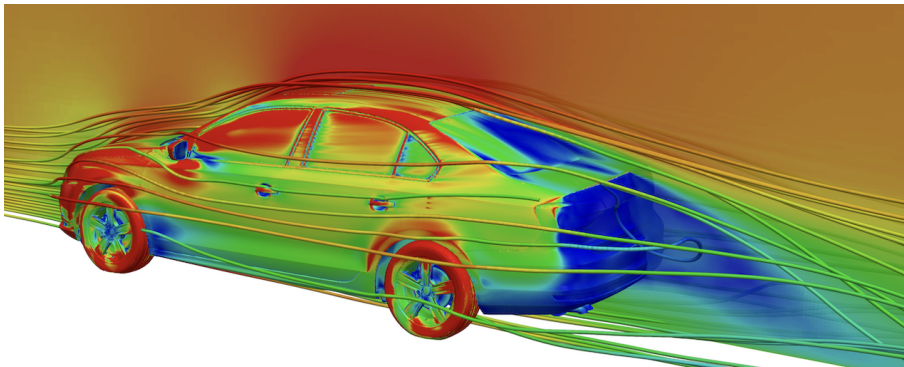


Figure 5: Visualization of the averaged flow field around the Jetta.

Table 1: Parameters' description of the Jetta-6 test case [32].

Parameter	Description	Lower bound	Upper bound
μ_1	Rear roof lowering	0 mm	50 mm
μ_2	Trunk height	-30 mm	30 mm
μ_3	Trunk length	-50 mm	100 mm
μ_4	Rear lateral tapering	-60 mm	50 mm
μ_5	Rear end edge position	-70 mm	30 mm
μ_6	Rear end depression	-15 mm	0 mm

The second automotive test case (named hereafter **Jetta-12**) is based on the same car model and was created within the EC project UPSCALE [1]. The parameterization consists of 12 geometric modifications all around the vehicle (see Figure 6 and Table 2). Besides the baseline geometry, a Sobol sequence of 300 additional samples was created and computed with OpenFOAM. To reduce the required computational budget to an affordable amount, Reynolds-Averaged-Navier-Stokes (RANS) computations were carried out instead of DDES runs. This allowed to use coarser meshes

of 52M cells and resulted in 1700 CPU-core-hours for a single run for the 4000 iterations, of which the last 1000 were averaged to obtain the drag coefficient c_D .

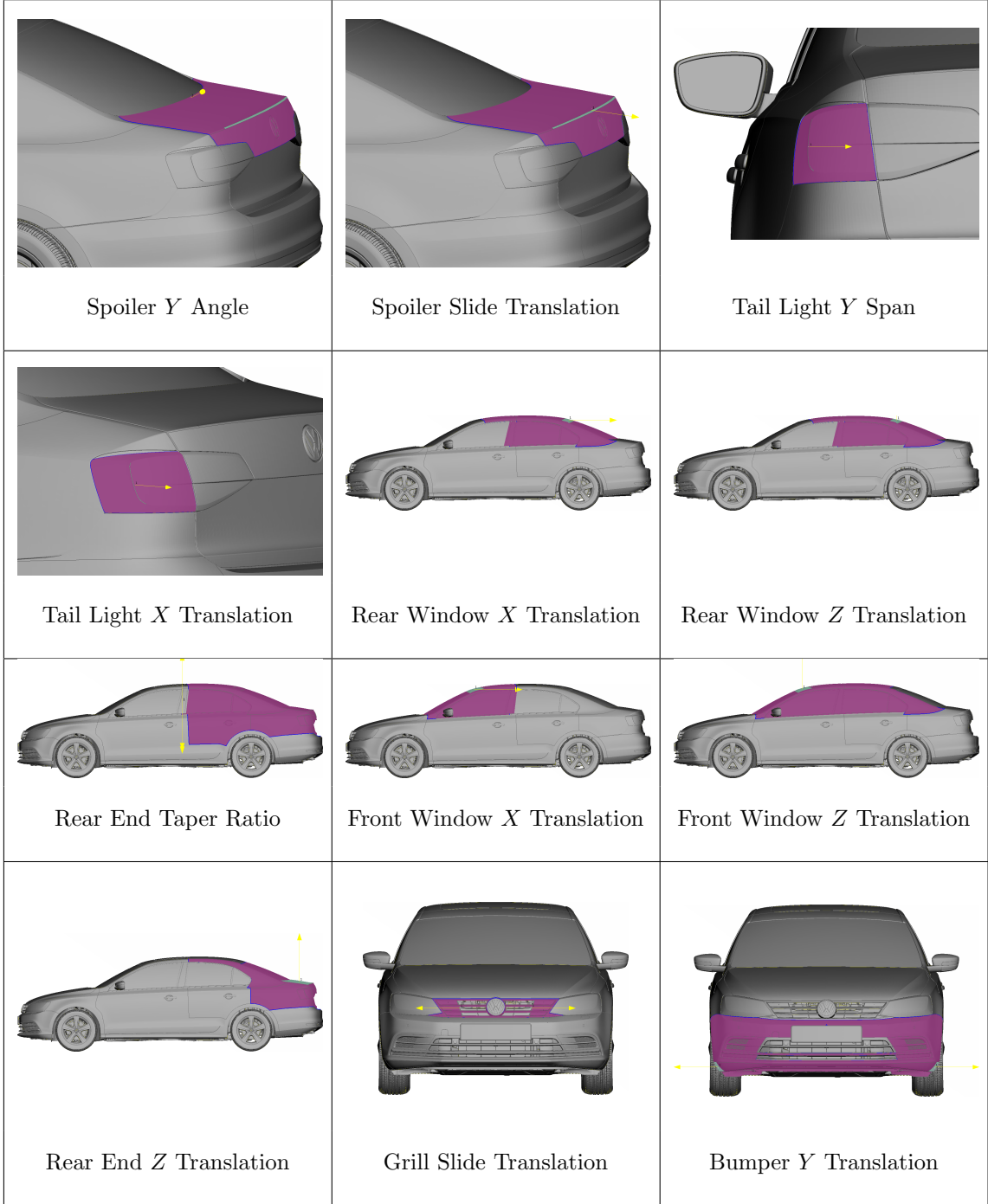


Figure 6: Affected areas by the geometrical parameters for the Jetta-12 test case. The ranges of each parameter can be gleaned from Table 2.

5.2.1 Multi-fidelity response surface design Jetta-6

In this test case, the low-fidelity model chosen is the response surface trained on the active latent variables obtained with the NLL method: instead of prolonging along the orthogonal directions the one-dimensional regression built on the active subspace, a GPR is trained on the deformed high-fidelity inputs $\{g_{\text{NLL}}(\mathbf{x}_i^H)\}_{i=1}^{N_H} \subset \tilde{\mathcal{X}}$. We remark that the map g_{NLL} does not preserve in general

Table 2: Parameters’ description of the Jetta-12 test case.

Parameter	Description	Lower bound	Upper bound
μ_1	Spoiler Y Angle	-5.0°	0.0°
μ_2	Spoiler Slide Translation	0.0 mm	30.0 mm
μ_3	Tail Light Y Span	-15.0 mm	5.0 mm
μ_4	Tail Light X Translation	-10.0 mm	10.0 mm
μ_5	Rear Window X Translation	-100.0 mm	100.0 mm
μ_6	Rear Window Z Translation	-30.0 mm	0.0 mm
μ_7	Rear End Taper Ratio	-1.0°	3.0°
μ_8	Front Window X Translation	-100.0 mm	100.0 mm
μ_9	Front Window Z Translation	-30.0 mm	0.0 mm
μ_{10}	Rear End Z Translation	-30.0 mm	30.0 mm
μ_{11}	Grill Slide Translation	-50.0 mm	50.0 mm
μ_{12}	Bumper Y Translation	-20.0 mm	20.0 mm

convexity of the domain \mathcal{X} or orthogonality of the boundaries. Nonetheless, this is not problematic for this application since we are not interested in backmapping the active latent variables from $\tilde{\mathcal{X}}$ to \mathcal{X} , but only in forwarding the inputs from \mathcal{X} to $\tilde{\mathcal{X}}$ and then evaluating the predictions with the GPR.

The RevNet employed has 10 layers. It was trained for 20000 epochs on a dataset of 76 training samples and 25 test samples, with ADAM stochastic optimization method [22], with an initial learning rate of 0.03. The high-fidelity samples were obtained with LHS method. The architecture is implemented in PyTorch [35] inside the ATHENA [42] Python package.

We perform a study on the number of additional LF samples, distributed uniformly on the domain, from 100 to 400 with a step of 50. The results are shown in Figure 7.

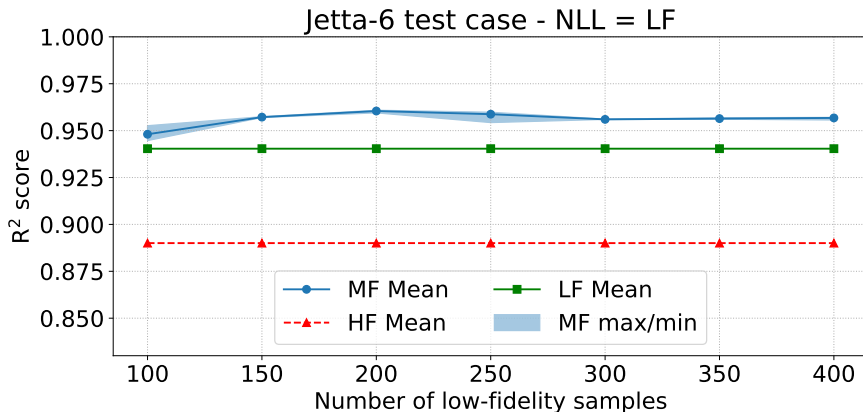


Figure 7: R^2 score evaluated on the 25 test samples obtained from LHS on the domain \mathcal{X} , varying the number of LF samples. The mean R^2 score over 10 restarts of the training of the GPR is shown. For the MF also the minimum and maximum values are shown. The LF and HF R^2 scores are reported, even though the LF and HF models are not influenced by the number of additional LF samples.

The maximization of the log-likelihood is performed with 10 restarts for the HF and LF models, and 100 restarts for the MF model, all inside GPy optimization algorithm. All training procedures are moreover restarted 10 times, testing the stability of the optimization process for each fidelity model. This is done in order to show, in Figure 7, that the MF training presents some small instabilities with respect to the HF and LF training, as expected. The LF and HF models are designed over the same HF inputs-outputs datasets, so they are not influenced by the additional LF samples.

Remark 3 (Reversing the fidelities order). A natural question that may arise regards the correct

ordering of the HF and LF models in the MF when the accuracy is higher for the LF as in Figure 7. We perform a study with respect to the number of additional samples from the HF GPR (nor from the numerical simulations), now the lowest fidelity in the MF model. Moreover in order to reach a desirable accuracy as in Figure 7, we add to each of the 2 levels of fidelity of the MF model 200 uniformly sampled input-output pairs: the highest fidelity is the NLL GPR built with $76 + 200$ training data; the lowest fidelity is the HF GPR built with training data equal to 76 from numerical simulations +200 fictitiously from the HR GPR (not from numerical simulations) + additional samples from 100 to 400 with a step of 50 from HR GPR (not numerical simulations). The results are reported in Figure 8. The R^2 score is lower than the previous case. Generally, the ordering of the fidelities depends on the availability of data and the cost for obtaining them.

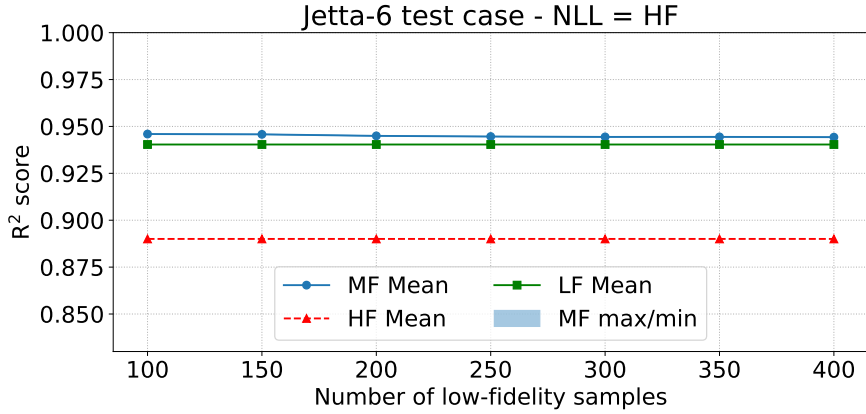


Figure 8: R^2 score evaluated on the 25 test samples obtained from LHS on the domain \mathcal{X} , varying the number of LF samples, which in this case is the HF GPR. The NLL GPR (LF) and HF GPR (HF) R^2 scores are shown, even though the LF and HF models are not influenced by the number of additional LF samples.

We also perform cross-validation (CV) with leave-one-out strategy for the Jetta-6 test case to assess the robustness of the result with respect to the test dataset, in Figure 9. We reported the mean and confidence intervals at 95% among the 25 batches of the leave-one-out strategy for a test set of 25 samples: each batch has 24 test samples. For each abscissa, the batches corresponding to the lowest R^2 score for the MF and highest R^2 score for the LF are found, so that with respect to these two selected batches the R^2 scores of the LF and MF models, respectively, can be computed and compared: we want to remark that batch-wise the MF R^2 score is always higher to the LF R^2 score.

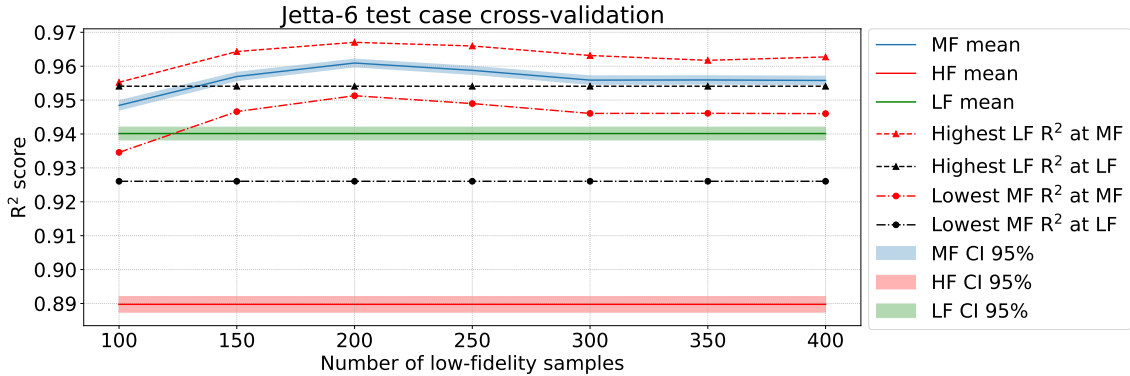


Figure 9: Cross-validation with leave-one-out strategy and confidence bounds at 95%. The labels **lowest MF R^2 at LF** stands for the R^2 score of the batch associated to the lowest R^2 score for the MF model in the CV procedure, but evaluated at the predictions of the LF model. The other labels are analogue.

5.2.2 Multi-fidelity response surface design Jetta-12

For this test case with additional 6 parameters with respect to the previous one, for a total of 12, a one-dimensional NLL response surface does not perform better than a one-dimensional AS response surface, so we preferred the latter as LF model. In this case we added also noise at each fidelity level in order to achieve a better accuracy, but loosing the Markov property, see Remark 2.

We perform a study on the number of high-fidelity samples from 45 to 225, obtained as a Sobol' sequence. The test set has 51 samples obtained with LHS instead. The number of additional LF samples is 100. The results are reported in Figure 10. As for the Jetta-6 test case, we show the average of the 10 outer training restarts for the MF, HF and LF models. In the case of the MF model we show also the maximum and minimum. Moreover the optimization procedures of the GPRs are restarted 10 times for the HF and LF models, and 100 times for the MF model.

It can be seen a gain of around 10% on the R^2 score of the MF model, with respect to the other two. This time the procedure is much less stable with respect to the optimization process, probably due to the higher dimension of the input space. The decreasing behaviour of the R^2 score of the HF and LF models from the abscissa 115 to 225 can be ascribed to the scarce test dataset with respect to the parameter space dimension and problem complexity.

We want also to remark that in this test case the training of the MF model takes from 4 to 10 minutes on average (depending on the number of HF samples from 75 to 225) relative to 100 GPy restarts of the GPR training, that is 100 for the first fidelity and another 100 for the second fidelity. The training takes less than 1 second for the HF and LF models (100 GPy restarts of the GPR training). Anyway confronted with the costs for a high-fidelity simulation, the MF training cost is negligible.

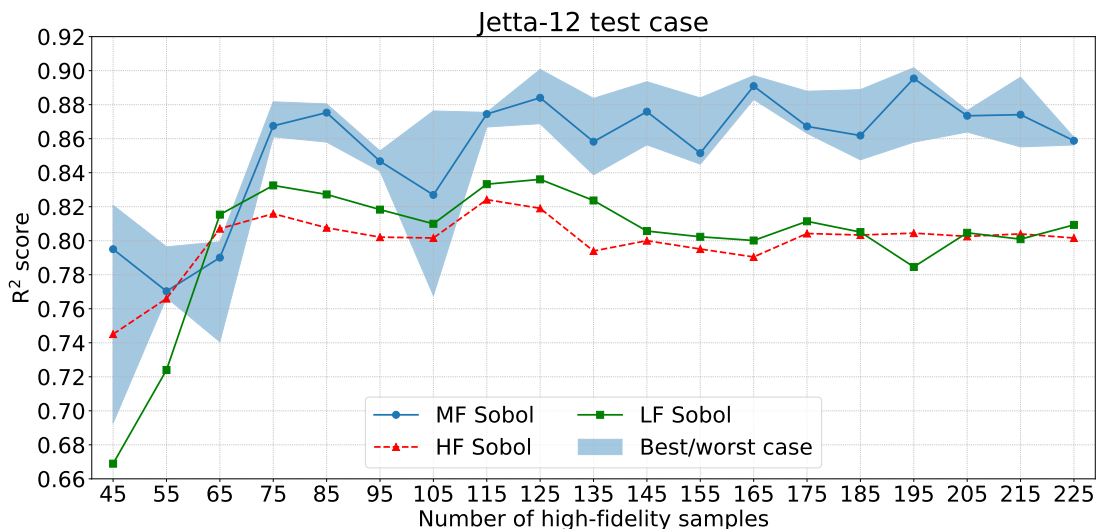


Figure 10: R^2 score evaluated on the 51 test samples obtained from LHS on the domain \mathcal{X} , varying the number of HF samples. The mean R^2 score over 10 restarts of the training of the GPR is shown. For the MF model the minimum and maximum values are shown, differently from the HF and LF models, since the perturbations are not sensible.

Also in this case we perform cross-validation with leave-one-out strategy for the Jetta-12 test case in Figure 11. We reported the mean and confidence intervals at 95% among the 51 batches of the leave-one-out strategy for a test set of 51 samples: each batch has 50 test samples. As for the Jetta-6 test case, for each abscissa, the batches corresponding to the lowest R^2 score for the MF and highest R^2 score for the LF are found, so that with respect to these two selected batches the R^2 scores of the LF and MF models, respectively, is computed. We remark that batch-wise the MF R^2 score is always higher to the LF R^2 score.

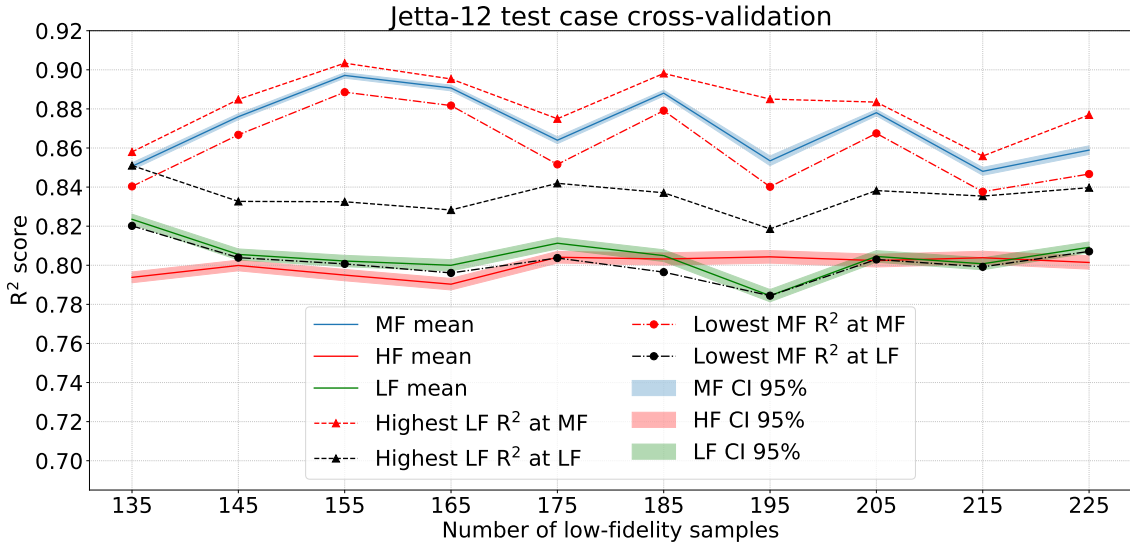


Figure 11: Cross-validation (CV) with leave-one-out strategy and confidence bounds at 95%. The labels **lowest MF R² at LF** stands for the R^2 score of the batch associated to the lowest R^2 score for the MF model in the CV procedure, but evaluated at the predictions of the LF model. The other labels are analogue.

6 Conclusions and future perspectives

In this work we propose a nonlinear multi-fidelity approach for the approximation of scalar functions with low intrinsic dimensionality. Such dimension is identified by searching for the existence of an active subspace for the function of interest or by employing the NLL method. With a regression along the active variable we build a low-fidelity model over the full parameter space which is fast to evaluate and does not need any new simulation. We just extract new information from the high-fidelity data we already have. This multi-fidelity approach results in an increased R^2 score and improved approximation capabilities over all the parameter space.

We apply the multi-fidelity with AS method to two different benchmark problems involving high dimensional scalar functions with an active subspace. We achieve promising results with a relative gain on the R^2 score around 3–5% with respect to the high-fidelity regression in one case (piston) and around 3–4% in the other one (Ebola), depending on the number of high-fidelity samples used. More remarkable results are obtained for less accurate high-fidelity models like the Jetta-12 test case: in this case we reached a relative gain on the R^2 score around 10%. For the Jetta-6 test case the relative gain is around 2% on the R^2 score with respect to the low-fidelity model and around 10% with respect to the high-fidelity model; this time the low-fidelity model is obtained from the NLL method.

Further investigations could involve the use of different fidelities based on extensions of AS, such as kernel active subspaces [40], or local active subspaces [41]. This could also greatly improve data-driven non-intrusive reduced order methods [44, 45, 46] through modal coefficients reconstruction and prediction for parametric problems [52]. We also mention the possible application to shape optimization problems for the evaluation of both the target function and the constraints.

Mandatory for real applications is a model management strategy providing theoretical guarantees and establishing accuracy and/or convergence of outer-loop applications. Some attempts towards multi-source Bayesian optimization/Experimental design are being studied. Moreover increasing the number of fidelities in the multi-fidelity model is a possible direction of investigation, especially when the phenomenon of interest allows many cheap low-fidelity approximations.

Acknowledgements

This work was partially supported by the European Commission H2020 ARIA (Accurate ROMs for Industrial Applications) project, by an industrial Ph.D. grant sponsored by Fincantieri S.p.A. (IRONTH Project), by MIUR (Italian ministry for university and research) through FARE-X-

AROMA-CFD project, by the European Commission H2020 UPSCALE project (Upscaling product development simulation capabilities exploiting artificial intelligence for electric vehicles, 824306), and partially funded by European Union Funding for Research and Innovation — Horizon 2020 Program — in the framework of European Research Council Executive Agency: H2020 ERC CoG 2015 AROMA-CFD project 681447 “Advanced Reduced Order Methods with Applications in Computational Fluid Dynamics” P.I. Professor Gianluigi Rozza.

References

- [1] Upscale (upsaling product development simulation capabilities exploiting artificial intelligence for electric vehicles). <https://www.upscaleproject.eu/>, 2021. [Online; accessed 2021-10-13].
- [2] E. N. Ben-Ari and D. M. Steinberg. Modeling data from computer experiments: an empirical comparison of kriging with MARS and projection pursuit regression. *Quality Engineering*, 19(4):327–338, 2007. doi:10.1080/08982110701580930.
- [3] L. Bonfiglio, P. Perdikaris, S. Brizzolara, and G. Karniadakis. Multi-fidelity optimization of super-cavitating hydrofoils. *Computer Methods in Applied Mechanics and Engineering*, 332:63–85, 2018. doi:10.1016/j.cma.2017.12.009.
- [4] L. Bonfiglio, P. Perdikaris, G. Vernengo, J. S. de Medeiros, and G. Karniadakis. Improving SWATH Seakeeping Performance using Multi-Fidelity Gaussian Process and Bayesian Optimization. *Journal of Ship Research*, 62(4):223–240, 2018. doi:10.5957/JOSR.11170069.
- [5] R. A. Bridges, A. D. Gruber, C. Felder, M. Verma, and C. Hoff. Active manifolds: A non-linear analogue to active subspaces. *arXiv preprint arXiv:1904.13386*, 2019.
- [6] B. Chang, L. Meng, E. Haber, L. Ruthotto, D. Begert, and E. Holtham. Reversible architectures for arbitrarily deep residual neural networks. In *Proceedings of the AAAI Conference on Artificial Intelligence*, volume 32, 2018.
- [7] P. G. Constantine. *Active subspaces: Emerging ideas for dimension reduction in parameter studies*, volume 2 of *SIAM Spotlights*. SIAM, 2015. doi:10.1137/1.9781611973860.
- [8] P. G. Constantine and P. Diaz. Global sensitivity metrics from active subspaces. *Reliability Engineering & System Safety*, 162:1–13, 2017. doi:10.1016/j.res.2017.01.013.
- [9] A. Damianou and N. Lawrence. Deep Gaussian processes. In *Artificial Intelligence and Statistics*, pages 207–215, 2013.
- [10] N. Demo, M. Tezzele, A. Mola, and G. Rozza. Hull Shape Design Optimization with Parameter Space and Model Reductions, and Self-Learning Mesh Morphing. *Journal of Marine Science and Engineering*, 9(2):185, 2021. doi:10.3390/jmse9020185.
- [11] N. Demo, M. Tezzele, and G. Rozza. A non-intrusive approach for reconstruction of POD modal coefficients through active subspaces. *Comptes Rendus Mécanique de l’Académie des Sciences, DataBEST 2019 Special Issue*, 347(11):873–881, November 2019. doi:10.1016/j.crme.2019.11.012.
- [12] N. Demo, M. Tezzele, and G. Rozza. A Supervised Learning Approach Involving Active Subspaces for an Efficient Genetic Algorithm in High-Dimensional Optimization Problems. *SIAM Journal on Scientific Computing*, 43(3):B831–B853, 2021. doi:10.1137/20M1345219.
- [13] P. Diaz, P. Constantine, K. Kalmbach, E. Jones, and S. Pankavich. A modified SEIR model for the spread of Ebola in Western Africa and metrics for resource allocation. *Applied Mathematics and Computation*, 324:141–155, 2018. doi:10.1016/j.amc.2017.11.039.
- [14] A. I. Forrester, A. Sóbester, and A. J. Keane. Multi-fidelity optimization via surrogate modelling. *Proceedings of the Royal Society A: Mathematical, Physical and Engineering Sciences*, 463(2088):3251–3269, 2007. doi:10.1098/rspa.2007.1900.

- [15] S. F. Ghoreishi, S. Friedman, and D. L. Allaire. Adaptive Dimensionality Reduction for Fast Sequential Optimization With Gaussian Processes. *Journal of Mechanical Design*, 141(7):071404, 2019. doi:10.1115/1.4043202.
- [16] GPy. GPy: A Gaussian process framework in Python. <http://github.com/SheffieldML/GPy>, since 2012.
- [17] A. Gruber, M. Gunzburger, L. Ju, Y. Teng, and Z. Wang. Nonlinear level set learning for function approximation on sparse data with applications to parametric differential equations. *arXiv preprint arXiv:2104.14072*, 2021.
- [18] E. Haber and L. Ruthotto. Stable architectures for deep neural networks. *Inverse problems*, 34(1):014004, 2017. doi:10.1088/1361-6420/aa9a90.
- [19] J. L. Jefferson, J. M. Gilbert, P. G. Constantine, and R. M. Maxwell. Active subspaces for sensitivity analysis and dimension reduction of an integrated hydrologic model. *Computers & Geosciences*, 83:127–138, 2015. doi:10.1016/j.cageo.2015.07.001.
- [20] M. Kanagawa, P. Hennig, D. Sejdinovic, and B. K. Sriperumbudur. Gaussian processes and kernel methods: A review on connections and equivalences. *arXiv preprint arXiv:1807.02582*, 2018.
- [21] M. C. Kennedy and A. O’Hagan. Predicting the output from a complex computer code when fast approximations are available. *Biometrika*, 87(1):1–13, 2000.
- [22] D. P. Kingma and J. Ba. Adam: A method for stochastic optimization. In *International Conference on Learning Representations (ICLR)*, 2015.
- [23] B. Kramer, A. N. Marques, B. Peherstorfer, U. Villa, and K. Willcox. Multifidelity probability estimation via fusion of estimators. *Journal of Computational Physics*, 392:385–402, 2019. doi:10.1016/j.jcp.2019.04.071.
- [24] R. R. Lam, O. Zahm, Y. M. Marzouk, and K. E. Willcox. Multifidelity Dimension Reduction via Active Subspaces. *SIAM Journal on Scientific Computing*, 42(2):A929–A956, 2020. doi:10.1137/18M1214123.
- [25] M. Lázaro-Gredilla, J. Quiñero-Candela, C. E. Rasmussen, and A. R. Figueiras-Vidal. Sparse spectrum Gaussian process regression. *The Journal of Machine Learning Research*, 11:1865–1881, 2010.
- [26] M. Lázaro-Gredilla and M. K. Titsias. Variational Heteroscedastic Gaussian Process regression. In *Proceedings of the 28th International Conference on International Conference on Machine Learning*, ICML’11, pages 841–848, Madison, WI, USA, 2011. Omnipress.
- [27] L. Le Gratiet and J. Garnier. Recursive co-kriging model for design of computer experiments with multiple levels of fidelity. *International Journal for Uncertainty Quantification*, 4(5):365–386, 2014. doi:10.1615/Int.J.UncertaintyQuantification.2014006914.
- [28] H. Liu, Y.-S. Ong, X. Shen, and J. Cai. When Gaussian process meets big data: A review of scalable GPs. *IEEE Transactions on Neural Networks and Learning Systems*, 2020.
- [29] T. W. Lukaczyk, P. Constantine, F. Palacios, and J. J. Alonso. Active subspaces for shape optimization. In *10th AIAA multidisciplinary design optimization conference*, page 1171, 2014. doi:10.2514/6.2014-1171.
- [30] X. Meng and G. E. Karniadakis. A composite neural network that learns from multi-fidelity data: Application to function approximation and inverse PDE problems. *Journal of Computational Physics*, 401:109020, 2020. doi:10.1016/j.jcp.2019.109020.
- [31] A. Mola, M. Tezzele, M. Gadalla, F. Valdenazzi, D. Grassi, R. Padovan, and G. Rozza. Efficient reduction in shape parameter space dimension for ship propeller blade design. In R. Bensow and J. Ringsberg, editors, *Proceedings of MARINE 2019: VIII International Conference on Computational Methods in Marine Engineering*, pages 201–212, 2019.

- [32] M. Mrosek, C. Othmer, and R. Radespiel. Reduced-order modeling of vehicle aerodynamics via proper orthogonal decomposition. *SAE International Journal of Passenger Cars — Mechanical Systems*, 12:225–236, 10 2019. doi:10.4271/06-12-03-0016.
- [33] C. Othmer, T. W. Lukaczyk, P. Constantine, and J. J. Alonso. On active subspaces in car aerodynamics. In *17th AIAA/ISSMO Multidisciplinary Analysis and Optimization Conference*, page 4294, 2016. doi:10.2514/6.2016-4294.
- [34] A. Paleyes, M. Pullin, M. Mahsereci, N. Lawrence, and J. González. Emulation of physical processes with Emukit. In *Second Workshop on Machine Learning and the Physical Sciences, NeurIPS*, 2019.
- [35] A. Paszke, S. Gross, F. Massa, A. Lerer, J. Bradbury, G. Chanan, T. Killeen, Z. Lin, N. Gimelshein, L. Antiga, A. Desmaison, A. Kopf, E. Yang, Z. DeVito, M. Raison, A. Tejani, S. Chilamkurthy, B. Steiner, L. Fang, J. Bai, and S. Chintala. Pytorch: An imperative style, high-performance deep learning library. In H. Wallach, H. Larochelle, A. Beygelzimer, F. d'Alché-Buc, E. Fox, and R. Garnett, editors, *Advances in Neural Information Processing Systems 32*, pages 8024–8035. Curran Associates, Inc., 2019.
- [36] P. Perdikaris, M. Raissi, A. Damianou, N. D. Lawrence, and G. E. Karniadakis. Nonlinear information fusion algorithms for data-efficient multi-fidelity modelling. *Proceedings of the Royal Society A*, 473(2198):20160751, 2017. doi:10.1098/rspa.2016.0751.
- [37] J. Quinonero-Candela, C. E. Rasmussen, and C. K. Williams. Approximation methods for Gaussian process regression. In *Large-scale kernel machines*, pages 203–223. MIT Press, 2007.
- [38] M. Raissi, P. Perdikaris, and G. E. Karniadakis. Inferring solutions of differential equations using noisy multi-fidelity data. *Journal of Computational Physics*, 335:736–746, 2017. doi:10.1016/j.jcp.2017.01.060.
- [39] M. Raissi, P. Perdikaris, and G. E. Karniadakis. Physics-informed neural networks: A deep learning framework for solving forward and inverse problems involving nonlinear partial differential equations. *Journal of Computational Physics*, 378:686–707, 2019. doi:10.1016/j.jcp.2018.10.045.
- [40] F. Romor, M. Tezzele, A. Lario, and G. Rozza. Kernel-based Active Subspaces with application to CFD parametric problems using Discontinuous Galerkin method. *arXiv preprint arXiv:2008.12083*, 2020.
- [41] F. Romor, M. Tezzele, and G. Rozza. A local approach to parameter space reduction for regression and classification tasks. *arXiv preprint arXiv:2107.10867*, 2021.
- [42] F. Romor, M. Tezzele, and G. Rozza. ATHENA: Advanced Techniques for High dimensional parameter spaces to Enhance Numerical Analysis. *Software Impacts*, page 100133, 2021. doi:10.1016/j.simpa.2021.100133.
- [43] F. Romor, M. Tezzele, and G. Rozza. Multi-fidelity data fusion for the approximation of scalar functions with low intrinsic dimensionality through active subspaces. In *Proceedings in Applied Mathematics & Mechanics*, volume 20. Wiley Online Library, 2021. doi:10.1002/pamm.202000349.
- [44] G. Rozza, M. Hess, G. Stabile, M. Tezzele, and F. Ballarin. Basic Ideas and Tools for Projection-Based Model Reduction of Parametric Partial Differential Equations. In P. Benner, S. Grivet-Talocia, A. Quarteroni, G. Rozza, W. H. A. Schilders, and L. M. Silveira, editors, *Model Order Reduction*, volume 2, chapter 1, pages 1–47. De Gruyter, Berlin, Boston, 2020. doi:10.1515/9783110671490-001.
- [45] G. Rozza, M. H. Malik, N. Demo, M. Tezzele, M. Girfoglio, G. Stabile, and A. Mola. Advances in Reduced Order Methods for Parametric Industrial Problems in Computational Fluid Dynamics. In R. Owen, R. de Borst, J. Reese, and P. Chris, editors, *ECCOMAS ECFD 7 - Proceedings of 6th European Conference on Computational Mechanics (ECCM 6) and 7th European Conference on Computational Fluid Dynamics (ECFD 7)*, pages 59–76, Glasgow, UK, 2018.

- [46] F. Salmoiraghi, F. Ballarin, G. Corsi, A. Mola, M. Tezzele, and G. Rozza. Advances in geometrical parametrization and reduced order models and methods for computational fluid dynamics problems in applied sciences and engineering: Overview and perspectives. *ECCOMAS Congress 2016 - Proceedings of the 7th European Congress on Computational Methods in Applied Sciences and Engineering*, 1:1013–1031, 2016. doi:10.7712/100016.1867.8680.
- [47] E. Snelson, Z. Ghahramani, and C. E. Rasmussen. Warped Gaussian processes. In S. Thrun, L. Saul, and B. Schölkopf, editors, *Advances in Neural Information Processing Systems*, volume 16, pages 337–344. MIT Press, 2004.
- [48] M. Tezzele, F. Ballarin, and G. Rozza. Combined parameter and model reduction of cardiovascular problems by means of active subspaces and POD-Galerkin methods. In D. Boffi, L. F. Pavarino, G. Rozza, S. Scacchi, and C. Vergara, editors, *Mathematical and Numerical Modeling of the Cardiovascular System and Applications*, volume 16 of *SEMA-SIMAI Series*, pages 185–207. Springer International Publishing, 2018. doi:10.1007/978-3-319-96649-6_8.
- [49] M. Tezzele, N. Demo, A. Mola, and G. Rozza. An integrated data-driven computational pipeline with model order reduction for industrial and applied mathematics. *Special Volume ECMI, Springer, In Press*, 2021.
- [50] M. Tezzele, N. Demo, G. Stabile, A. Mola, and G. Rozza. Enhancing CFD predictions in shape design problems by model and parameter space reduction. *Advanced Modeling and Simulation in Engineering Sciences*, 7(40), 2020. doi:10.1186/s40323-020-00177-y.
- [51] M. Tezzele, F. Salmoiraghi, A. Mola, and G. Rozza. Dimension reduction in heterogeneous parametric spaces with application to naval engineering shape design problems. *Advanced Modeling and Simulation in Engineering Sciences*, 5(1):25, Sep 2018. doi:10.1186/s40323-018-0118-3.
- [52] M. Tezzele, M. Sidari, M. Sicchiero, and G. Rozza. A multi-fidelity approach coupling parameter space reduction and non-intrusive POD with application to structural optimization of passenger ship hulls. Submitted, 2021.
- [53] H. G. Weller, G. Tabor, H. Jasak, and C. Fureby. A tensorial approach to computational continuum mechanics using object-oriented techniques. *Computers in physics*, 12(6):620–631, 1998. doi:10.1063/1.168744.
- [54] C. K. Williams and C. E. Rasmussen. *Gaussian Processes for Machine Learning*. Adaptive Computation and Machine Learning series. MIT press Cambridge, MA, 2006.
- [55] O. Zahm, P. G. Constantine, C. Prieur, and Y. M. Marzouk. Gradient-based dimension reduction of multivariate vector-valued functions. *SIAM Journal on Scientific Computing*, 42(1):A534–A558, 2020. doi:10.1137/18M1221837.
- [56] G. Zhang, J. Zhang, and J. Hinkle. Learning nonlinear level sets for dimensionality reduction in function approximation. In *Advances in Neural Information Processing Systems*, pages 13199–13208, 2019.